The International Journal of Advanced Manufacturing Technology (2022) 122:377–390
https://doi.org/10.1007/s00170-022-09528-y

ORIGINAL ARTICLE

# Dynamic simulation and experimental study of cutting force by rake angle of multi-axis high-speed ball-end milling tool

**Zhijie Wang[1] · Yan Cao[1] · Hui Yao[1] · Fan Kou[1]**

Received: 17 February 2022 / Accepted: 13 June 2022 / Published online: 19 July 2022


## Abstract

Aluminum alloy high-speed milling is commonly utilized in the aircraft, aerospace, mold, and other sectors, and its cutting force characteristics will have an important impact on the final machining quality of parts. The cutting force characteristics of high-speed milling of an aluminum alloy workpiece using a ball end milling cutter were investigated in this research. A three-dimensional finite element dynamic simulation model was developed for the high-speed milling of ball-end milling cutters. Firstly, the benefit of tool axis vector inclination angle in multi-axis machining was discussed, and the inclination angle of the tool axis vector in multi-axis machining was characterized more precisely. The three-dimensional model of the ball-end milling cutter was established according to the actual machining, and in order to simulate the machining process, it was put into a finite element analysis system. The rotation and intermittent cutting of the tool were considered in the simulation process, which was in good agreement with the actual machining process. In a finite element simulation environment, the cutting force under 25 groups of rake inclination angles was simulated, and verification milling tests on a five-axis machine were carried out. According to the results, the general trend of the maximum cutting force in all directions was in good agreement with the experimental results. Finally, the range of the rake inclination angle with less cutting force and more stable cutting force in multi-axis machining was given. The results also confirmed the reliability of the simulation results, and provided a reference for the finite element simulation of other metal cutting processes.

**Keywords** Multi-axis machining · High-speed · Dynamical finite element simulation · Ball end milling · Rake angle · Cutting force

## 1 Introduction

In aerospace, vehicle manufacturing, mold processing, and the biomedical sector, multi-axis high-speed ball milling technology is extensively employed in the creation of complicated surface and multi-feature products [1, 2]. Its process analysis, simulation model establishment, geometric simulation, and physical simulation are of great significance to the machining quality and accuracy of parts. The cutting force in physical simulation directly affects the cutting power, cutting heat, workpiece deformation, and vibration [3, 4]. As a result, precise cutting force prediction becomes a critical aspect of machining performance improvement. In the multi-axis ball milling process, the inclination angle of the tool axis vector is closely related to the prediction of cutting force, and the inclination angle of the tool axis vector has a significant impact on tool vibration and workpiece deformation, so it is necessary to investigate the influence of tool axis vector inclination on cutting force and simulation [5].

Cutting force modeling is the core of numerical control (NC) machining process, and the precondition of deformation and surface morphology of machining is the focus of many scholars. Wan et al. [6] thought that tool runout had a significant impact on the amount and distribution of cutting force. Kao et al. [7] suggested a technique of cutting force coefficient calculation based on stable milling settings, believing that the influence of the tool helix angle should be included in the calibration of the cutting force coefficient. Different from the research methods of other scholars,

This article is part of the Topical Collection: *New Intelligent Manufacturing Technologies through the Integration of Industry 4.0 and Advanced Manufacturing*

✉ Yan Cao
670533578@qq.com

[1] Mechanical and Electrical Engineering, Xi'an Technological University, No. 2 Xuefu Middle Road, Xi'an, Shaanxi Province 710021, People's Republic of China

Zuperl et al. [8] used the method of artificial neural network algorithm and experiment to get a prediction model of cutting force of ball end milling cutter. The artificial neural network was trained by 3500 groups of experimental data. The results showed that the approach of neural network to the predicted value of three cutting force components and experimental value was 4%, while the prediction value of the analysis method was only 11%. Some scholars used the orthogonal cutting model [9], oblique cutting model [10], and cutting data model [11] to determine the cutting force coefficient, and some scholars have also considered the end effect and the tip radius effect [12].

The finite element simulation of cutting force is the basis of the research on NC machining process. The numerical simulation of parts milling process using finite element analysis technology is a favorable means to study the cutting process and analyze the cutting force. Ehmann et al. [13] analyzed the literatures about finite element simulation technology in cutting process from 1971 to 1995. There were two kinds of finite element models in the cutting process: Lagrangian models and Euler models. He believed that in order to deepen the to understand the cutting process, it is necessary to further study the damping during the cutting process, cutting model calibration, cutting process dynamics, and tool wear. Nishida et al. [14] created a new cutting force simulator that takes into account a variety of elements like the cutting edge, immediate workpiece shape, and uncut chip thickness. To forecast the cutting force in micro-face milling, Wang et al. [15] suggested a mechanical model that takes into consideration the machining system's geometric error and the cutting edge's trochoidal trajectory. In order to improve cutting force performance, Aydin et al. [16] established the finite element model of the cutting force of the wave tool, and verified that the cutting force performance of the wave tool was better than that of the standard tool. Yue et al. [17] summarized the latest research progress of cutting finite element simulation at home and abroad by introducing the importance of finite element simulation and its commonly used software and material constitutive model, and considered that finite element simulation technology played an irreplaceable role in quantitative research and process parameters of metal cutting process.

In multi-axis NC high-speed machining, ball-end milling cutter is an essential tool with complex geometry. When milling with a ball end-milling cutter, the inclination angle of the cutter axis vector has a significant impact on the cutting process and cutting force due to the high-speed machining. Ko et al. [18] simulated and evaluated 7 inclination inclinations (0°, 10°, 15°, 20°, 30°, 40°, 45°) to reduce tool wear. The results revealed that a 15° machine rising angle was the most effective. Different from the research of Ko et al. [18], Kang et al. [19] discussed the relationship between cutting speed and three-axis cutting force using the included angles of three inclined surfaces of 15°, 30°, and 45°. Cutting horizontally downward on a 15° inclined plane was not an acceptable machining procedure, according to the findings of the experiments. Subsequently, Cao et al. [20] put forward an experimental approach for determining the force coefficient while taking into account the inclination angle, as well as investigating the impact of the inclination angle on the cutting force. The cutting force was found to be significantly affected by the inclination angle between the tool and the workpiece, with the cutting force initially decreasing and then increasing as the inclination angle was increased. Azeem et al. [21] proposed an improved multi-axis ball-end milling machine cutting force prediction model, which considered the influence of horizontal, non-horizontal, and rotary cutting motion of the tool on the cutting force, and verified the effectiveness of the model through experiments. Nan et al. [22] proposed a new method for predicting cutting force in the ball-end milling process that took into account the entry and exit angles of cutting zones for different cutter layers, calibrated the cutting force coefficients of different cutting layers, and improved cutting force prediction accuracy. Although the inclination angle between tool and workpiece has been investigated in the literature above, the impact of the inclination angle on cutting force has been studied through prediction and experiment. However, there was no classified study on the inclination angle of the tool vector, and the range of the inclination angle studied was too small to represent the optimal range of the inclination angle; the spindle speed in the milling process was in the low-speed cutting area, which did not address the impact of the inclination angle on the cutting force in high-speed cutting.

The inclination angle between the tool and the workpiece in multi-axis milling was divided into forward rake angle and inclination angle in this study, and the impact of the forward rake angle on cutting force under high-speed milling conditions was investigated, with a finite element simulation model developed. At the same time, the simulation study of forward inclination angle in the range of 12–60° was carried out. Then, the experiment was carried out using an Al alloy 7075 material by changing the inclination angle of the workpiece. Finally, experiments are used to verify the simulation model's effectiveness. The simulation allowed for a better understanding of ball end milling with an inclination angle in the feed direction. The investigation also revealed the range of optimum inclination angles in feed direction.

## 2 Finite element dynamic simulation and analysis of cutting force based on Deform-3D

Metal milling is a complex dynamic physical process with strong thermal–mechanical coupling that involves elasticity, plasticity, fracture mechanics, but also thermodynamics, tribology, etc. So traditional analytical approaches make it difficult to quantitatively assess and study the cutting

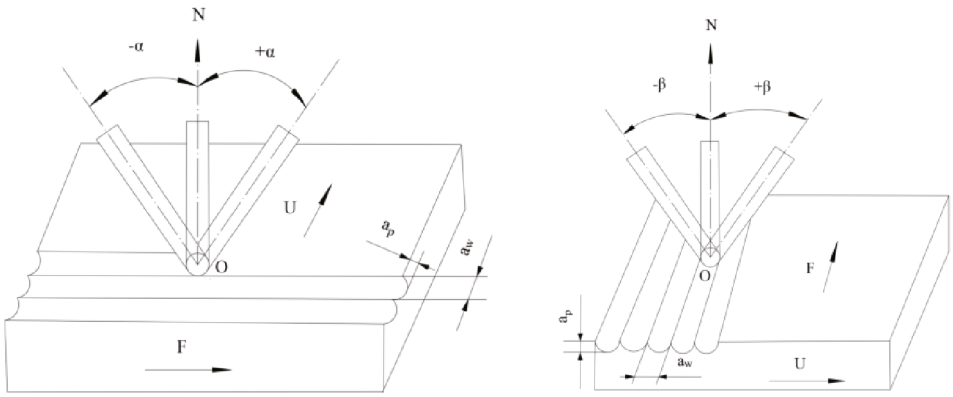


**(a)** Rake angle **(b)** Side inclination angle

**Fig. 1** Schematic diagram of vector inclination angle of tool axis. **a** Rake angle. **b** Side inclination angle

mechanism. It can effectively predict the chip shape, non-uniform stress field, strain field, and temperature field in the workpiece, tool, and chip under thermal and mechanical coupling, as well as the cutting force, tool wear, and residual stress on the workpiece's surface using numerical simulation technology, particularly the finite element method. Thus, the relationship model between cutting process parameters (machining path, cutting parameters, tool geometric parameters, clamping, etc.) and these physical parameters is established, and the process parameters are optimized.

## 2.1 Inclination angle of cutter shaft

Cutting force is one of the important indicators of the machinability of cutting during the milling of machined parts. Due to the effect of the cutting force, the part will be deformed during the machining process, and the deformation will affect the surface machining quality. Therefore, the establishment of a correct, effective, calculable, and deal with the cutting force prediction model is a critical foundation for studying component machining deformation. In multi-axis machining, the cutting force is proportional to the tool axis' inclination angle. One of the most essential aspects of studying the surface machining quality of items is determining the influence of the tool axis inclination angle on the cutting force.

When the ball-end milling cutter is processing parts in five-axis machining, the cutting speed of the cutting edge at the cutting edge is 0, which is equivalent to the sliding friction of the cutting edge on the machined surface, assuming that the cutter axis vector is perpendicular to the surface of the workpiece. At this time, it is not a real cutting, but an extrusion. On the one hand, it will increase the cutting force sharply and reduce the manufacturing accuracy of the parts. On the other hand, it will also increase the friction between the tool and the parts and reduce the surface quality of the machined parts. Finally, because the strength of the ball end milling cutter tip is much lower than other parts, it will also accelerate tool wear and reduce tool life. Therefore, when using a ball-end milling cutter in the actual processing, the tool axis will be offset by a certain angle to avoid the tool tip. Thus, it can avoid cutting the workpiece surface directly and prevent interference and collision between the tool and the workpiece.

Tool axis vector inclination angle can be divided into rake angle $\alpha$ and side inclination angle $\beta$, as shown in Fig. 1. $F$ is the feed direction of the tool; $U$ is the row pitch direction of the tool path, that is, the offset direction of the tool

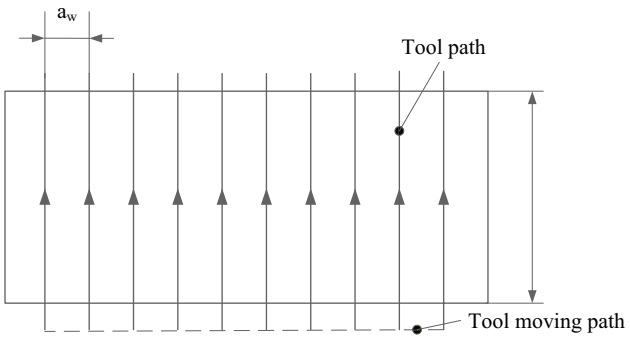


**Fig. 2** Cutter feed route of single direction milling

**Table 1** Geometry parameters of the ball end mill

| Geometrical parameters | Value |
|---|---|
| Radius of the ball end mill | 0.5 mm |
| Radius of tool shank | 2 mm |
| Taper angle of the ball end mill | 6° |
| Rake angle | 8° |
| Relief angle | 10° |
| Helical angle | 30° |
| Total length of the ball end mill | 60 mm |
| Length of cutting edge in axis direction | 15 mm |
| Number of teeth | 2 |

**Fig. 3** Cutter

**Fig. 4** The model of cutter

path; $N$ is the normal direction of the tool axis vector; $O$ is the center point of the tool; $a_p$ is the cutting depth of the tool, that is, the radial cutting depth; and $a_w$ is the cutting width of the tool, that is, the axial cutting depth. The rake angle $\alpha$ indicates that the tool axis vector tilts along the feed direction $F$ with the row pitch direction $U$ as the rotation axis. If the tilt direction of the tool axis vector is the same as the feed direction, then $\alpha$ is positive; the milling mode is pull milling; otherwise, $\alpha$ is negative, the milling mode is push milling. The side inclination angle $\beta$ means that the tool axis tilts along the row pitch direction $U$ with the feed direction $F$ as the rotation axis. If the tilt direction of the tool axis vector is consistent with the stepping direction, the $\beta$ is positive; otherwise, it is negative. It studies the influence of pull-milling mode on the cutting force when the forward inclination angle $\alpha$ is positive in this paper. At the same time, in order to highlight the influence of the rake angle on the cutting force, only the case of one-way feed of ball-end milling cutter is considered, as shown in Fig. 2.

## 2.2 Establishment of geometric model

The tool is a ball-end mill with a taper in this article, and the tool model is established by using 3D modeling software according to the tool structure size used in subsequent experiments, and the tool material is WC. For the part of the workpiece, in order to simulate the actual machining situation and obtain the expected analysis result, only the part close to the machined surface is selected as the analysis object. At the same time, it is considered that the tool is rigid in the analysis, and the tool rotates and feeds at the same time in the motion analysis. The inner surface of the workpiece imposes full constraints, so the motion process of milling is completely simulated. The geometric parameters of the tool are shown in Table 1, and the tool entity and geometric model are shown in Figs. 3 and 4.

## 2.3 Meshing technology

In the process of simulating metal cutting, mesh generation is one of the most important steps, especially for the model with complex geometry. The quality of mesh generation directly affects the solution accuracy and time. In the process of high-speed milling, the cutting layer of the workpiece is continuously deformed under the pushing action of the cutting edge of the cutter, which can distort the initial mesh and make the calculation difficult, cause the interruption of the solution process, or even unable to calculate.

Therefore, the ALE (arbitrary Lagrange-Euler) adaptive grid is used in the simulation process to maintain a high-quality grid and prevent the analysis and calculation from terminating due to severe grid deformation. In general, the finer the mesh, the more accurate the calculation results, but the amount of calculation will also increase significantly and the calculation time will be longer. In order to solve the problem, the high mesh density and curvature refinement of the chip area are used for mesh refinement and the mesh refinement of the chip formation area; that is, the dynamic local encryption function is used to adjust the tool tip, cutting layer, and the nearby local area, so that the mesh at the

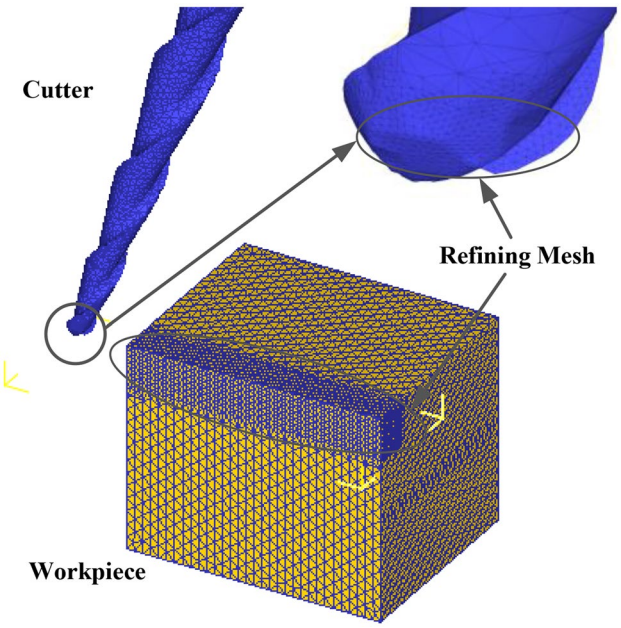


**Fig. 5** Simulation mesh

**Table 2** Chemical composition of Al7075-T6 alloy (%, mass fraction)

| Element | Zn | Mg | Si | Cr | Ti | Fe | Mn | Al |
|---|---|---|---|---|---|---|---|---|
| Assay | 5.83 | 2.37 | 0.05 | 0.22 | 0.03 | 0.07 | 0.04 | the rest |

stress concentration is finer, while the mesh far away from the machining part and the stress concentration is obviously looser. As the cutting process progresses, the dense grid area of the workpiece also shifts, presenting a dynamically changing grid adaptive division state. The grid divided in this way not only speeds up the simulation speed, but also prevents the distortion of the grid as the cutting process advances and affects the simulation accuracy.

The total number of tetrahedral elements on the cutter after mesh generation is 25,000, with a ratio of element size in the refined space to element size in the outer space of 0.001. For the sake of computational accuracy, the total number of tetrahedral elements on the workpiece is 50,000, and the ratio of element size in the refined space to element size in the outer space is 0.001, as shown in Fig. 5.

## 2.4 Establishment of tool and workpiece material model

The Al7075-T6 alloy, which contains zinc and magnesium components and is part of the Al–Zn–Mg–Cu class of extremely hard aluminum, was chosen for this study. Table 2 shows the chemical compositions in weight percent.

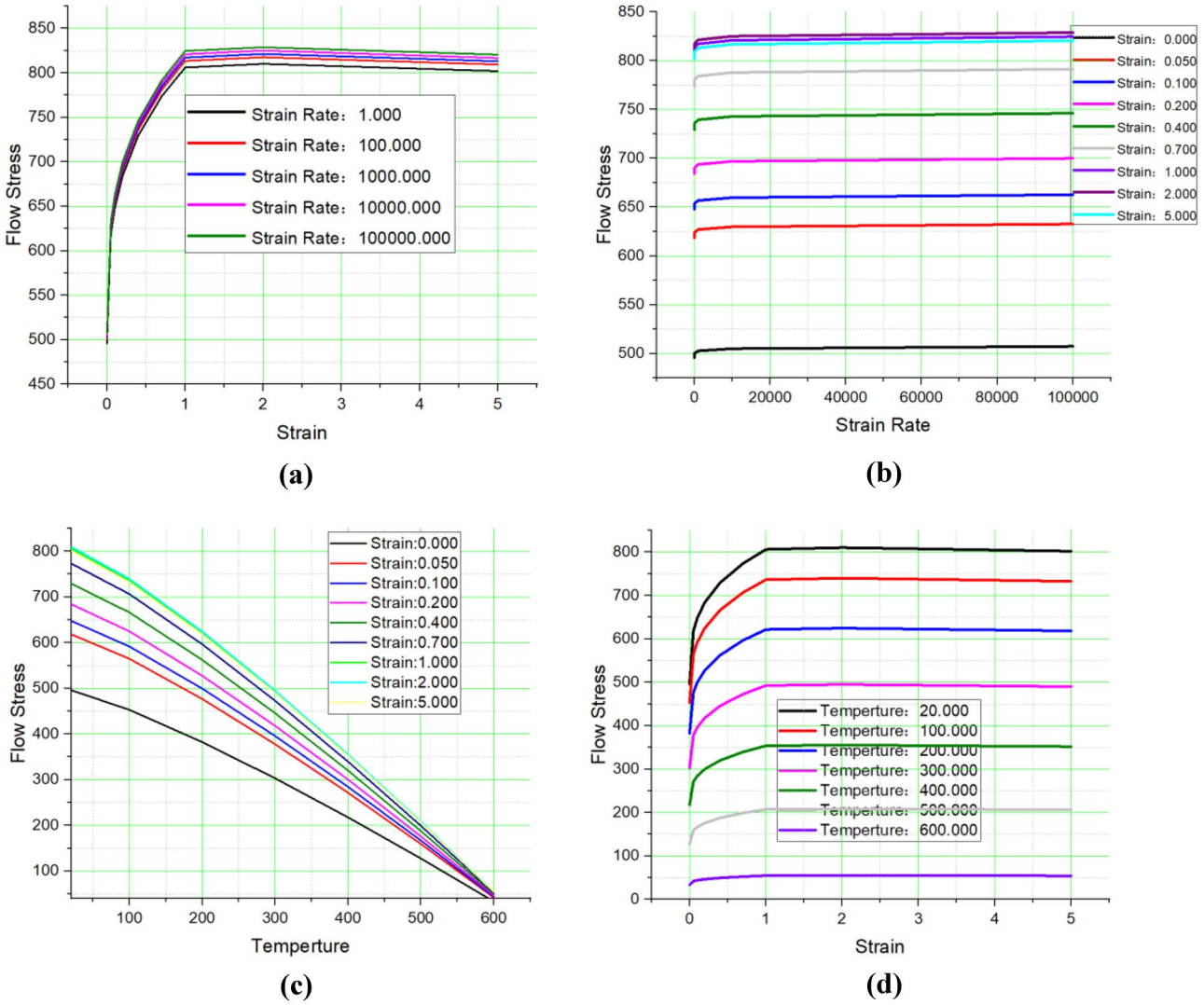


**Fig. 6** Flow stress of Al7075-T6 alloy at different strain, strain rate, and temperature comparison of flow stress

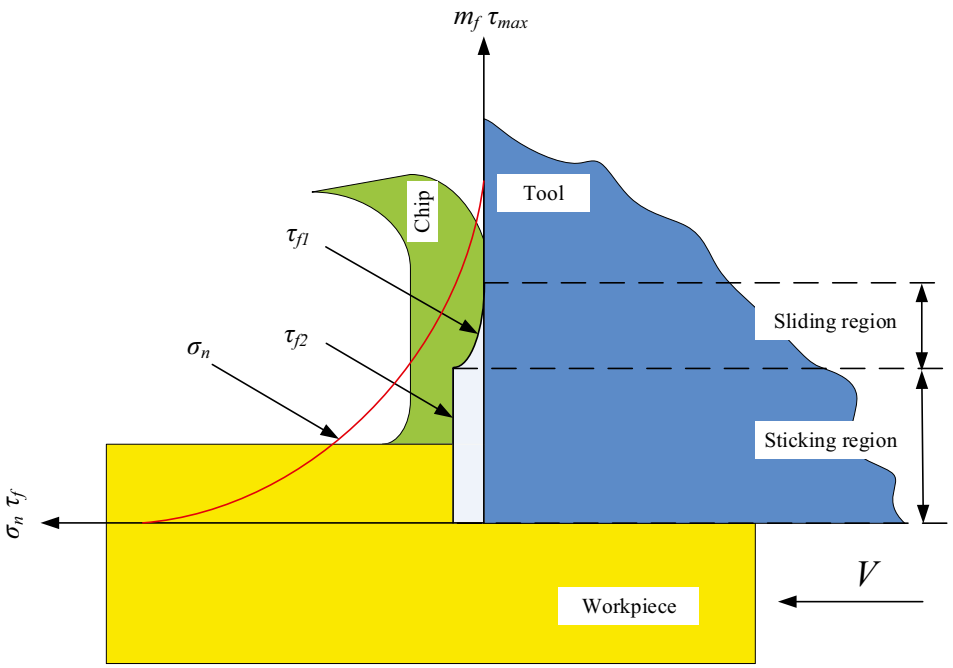


**Fig. 7** Curves representing normal and frictional stress distributions on a tool rake face in high-speed machining

It is necessary to understand the constitutive behavior of the material under these high-speed cutting conditions in order to use the finite element analysis numerical method to analyze the cutting process of aluminum alloy, so accurate flow stress data of the working material is required. In fact, the flow stress of the workpiece material determines the accuracy and reliability of the numerical model to a considerable extent, and the flow stress of the material is defined by the flow stress equation. It is vital to understand the constitutive behavior of the material under these high-speed cutting conditions in order to utilize the finite element analysis numerical method to study the cutting process of aluminum alloy; therefore, correct flow stress data of the working material is required. Indeed, the flow stress of the workpiece material is characterized by the flow stress equation, and the accuracy and reliability of the numerical model are heavily reliant on it. The basic formula expression form is:

$$\sigma = f(\varepsilon, \dot{\varepsilon}, T) \tag{1}$$

where:

$\varepsilon$ material strain;
$\dot{\varepsilon}$ material strain rate;
$T$ temperature.

Under different temperature conditions, the stress intensity of the plastic deformation of the material is different, and the stress–strain relationship is also different due to the different plastic deformation conditions of the material.

As a result, the mechanical analysis of the elastoplastic deformation process in high-speed metal machining must be done under actual deformation conditions. The flow stress curves of Al7075-T6 alloy strain from 0 to 5, strain rate from 0 to 100,000 $s^{-1}$, and beginning temperature from 20 to 600 °C are shown in Fig. 6a–d. The flow stress of Al7075-T6 alloy is observed to remain almost constant with increasing strain at a steady-state area, as can be seen by the progressive rise of the curves as the strain increases. This is because as the temperature

**Table 3** Simulation calculation conditions

| Workpiece material | Cutting tool | | Machining condition | |
|---|---|---|---|---|
| Al7075_T6 machining | Type | Taper ball-end milling cutter | $n$: spindle speed (rpm) | 20,000 |
| | | | $f$: feed speed (mm/s) | 50 |
| | Material | WC | $a_p$: cutting depth (mm) | 0.1 |
| | | | $a_w$: cutting width (mm) | 0.5 |
| | | | $\alpha$: rake angle (°) | 12 ~ 60 (simulation done every 2°) |

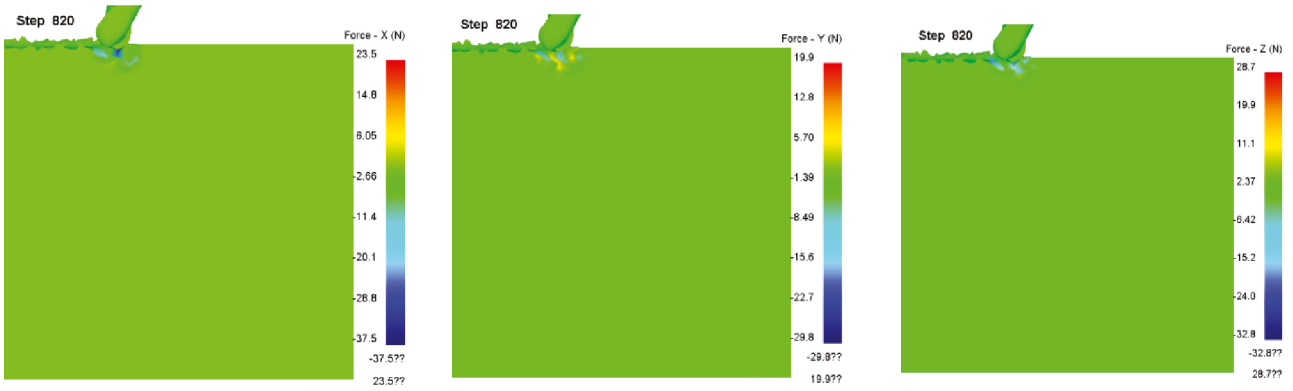


**(a)** X-direction force cloud atlas **(b)** Y-direction force cloud atlas **(c)** Z-direction force cloud atlas

**Fig. 8** Cloud atlas of force on the workpiece. **a** *X*-direction force cloud atlas. **b** *Y*-direction force cloud atlas. **c** *Z*-direction force cloud atlas

rises, the material recovers and recrystallizes, or softens, removing or partially removing the strain hardening effect.

The tool base material is WC cemented carbide, set as a rigid body. And the workpiece material is Al 7075-T6 machining, the density $\rho = 2810$ kg /m$^3$, elastic modulus $E = 71$GP, and Poisson's ratio $\mu = 0.33$. The yield function type is von Mises, and the hardening rule is isotropic.

## 2.5 Friction criterion

In the process of cutting, because of the extrusion and friction of the rake face of the tool, the flow rate of the material near the rake face gradually slows down. The heat generated by the friction aggravates the temperature rise of the chip contact surface. The cutting heat will directly affect tool wear and service life. The early cutting finite element simulations used the Coulomb friction criterion for the friction stress of the chip contact surface, but the criterion is only used for low-speed cutting. Because under high-speed cutting conditions, the chip flow rate on the rake face of the tool is quick, and the tool and chip contact area will generate a lot of contact stress and a lot of heat in a short time, which makes the friction mechanism in this area more complicated. The friction stress generated by the tool interface-chip contact area no longer follows the Coulomb friction criterion.

In the study of [23], not only the friction mechanism of high-speed cutting was considered, but also the shear friction coefficient was introduced to describe the friction in the bonding area. Based on the amount of deformation, calculate the normal stress at the interface. The normal stress $n$ of the site determines whether the contact point is in the sliding or adhesion zone, as shown in Fig. 7. Equation 4 below can be used to describe it mathematically. The modified Coulomb friction criterion was employed in this study, and the friction coefficient of the sliding friction zone was adjusted to 0.6, and the constant friction stress was applied in the adhesion zone, based on the actual contact state of the milling zone. In the numerical simulation, the friction of the adhesion zone, the coefficient is set to 1 (internal friction).

## 2.6 Selection of material chip separation and fracture criteria

The removal of workpiece material is accomplished in the numerical simulation of the ball-end milling process by the relative feed motion between the cutter and the workpiece, which causes a portion of the workpiece material to separate from the body to produce chips and a new cutting surface. The chip separation is based on the degree of mesh distortion in the calculation area caused by high temperature and large deformation of the material. The mesh of the calculation area with large distortion needs to be remeshed with the element adaptive meshing technology, so that the finite element analysis can be carried out. In this paper, Deform-3D default separation criterion is used; that is, when the tensile stress of the contact node between the workpiece and the chip that has not been separated is 10% greater than the compressive force, the node begins to separate, and the chip is separated.

**Table 4** Experimental equipment information

| Equipment | Experimental condition |
|---|---|
| Machine tool | JDGR200 A10SH five-axis high precision machining center |
| Cutting tool | φ1 mm carbide double-edge taper ball milling cutter without coating |
| Workpiece material | 7075-T6 Aluminum alloy |
| Milling force measuring equipment | 9257B Kistler dynamometer |
| Data acquisition card | HP3852S |
| Charge amplifier | 5070A |

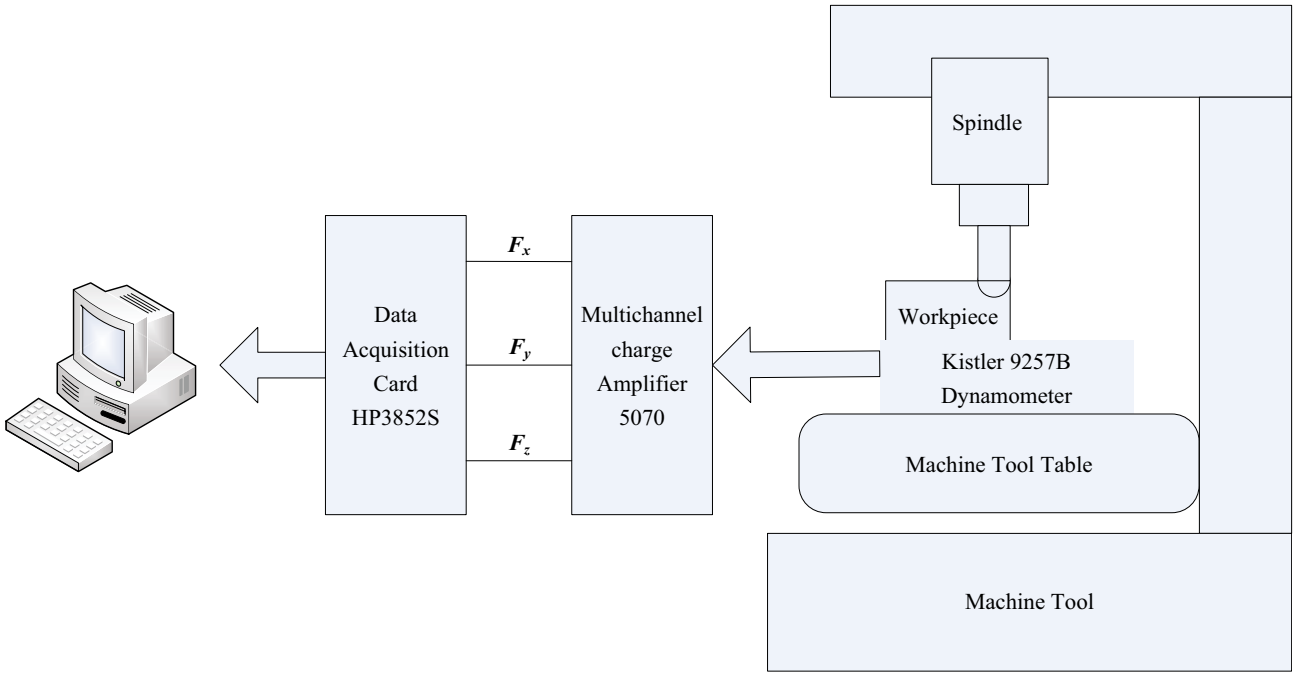


**Fig. 9** Principle of milling force measurement

The normalized Cockcroft and Latham fracture criterion [24] considers that chip fracture is mainly related to the tensile principal stress; that is, the material will fracture when the maximum tensile stress–strain energy reaches the critical failure value of the material at a certain temperature and strain rate. With great accuracy, the damage model has been applied to a variety of materials and processing methods. The normalized Cockcroft and Latham fracture criterion can be expressed as

$$C = \int_0^{\bar{\varepsilon}_f} \frac{\sigma_1}{\sigma} d\varepsilon \tag{2}$$

Where:

$C$ critical damage value;
$\bar{\varepsilon}_f$ equivalent plastic strain of the material at fracture;
$\sigma_1$ maximum principal stress at material fracture, MPa;
$\sigma$ equivalent stress, MPa.

## 2.7 Simulation calculation

The cutting process is a plastic problem with large deformation and presents a high geometric nonlinearity, so the cutting model is based on the updated Lagrange method,

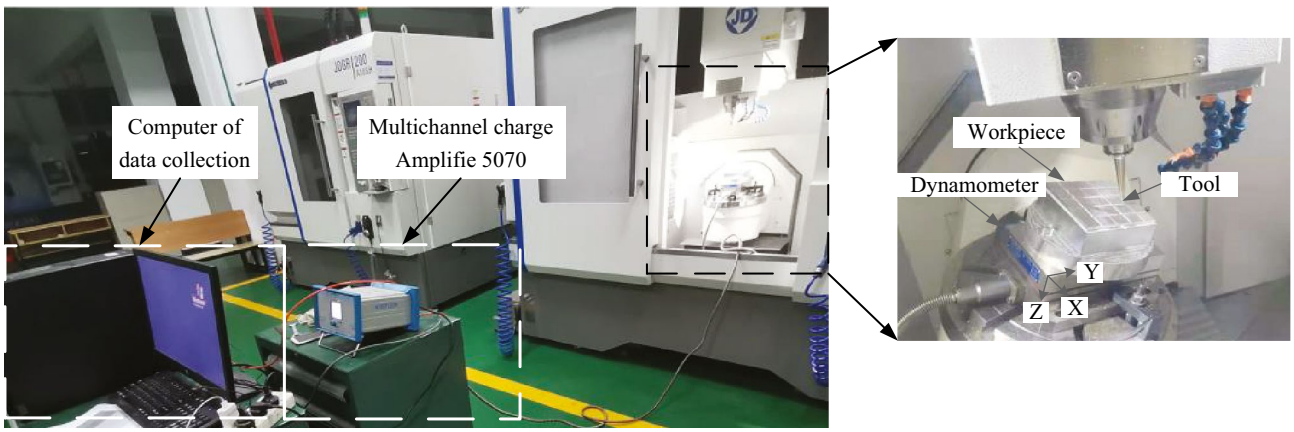


**Fig. 10** Experimental data measurement chart

which has the function of mesh adaptation and re-division. This research employs a modified Coulomb's law friction model, with a friction coefficient of 0.6 in the sliding friction area and constant friction stress in the adhesion area, based on the actual contact state of the milling area, and sets the friction coefficient of the bonding area to 1 (internal friction) in numerical simulation. The data of cutting force, interface temperature, and chip thickness can be easily obtained by simulation. The simulation conditions are shown in Table 3.

### 2.8 Simulation results and analysis

According to the finite element model, the milling process is simulated to obtain the changes of chip, workpiece stress and strain, temperature field, and cutting force during milling process. The rake angle of 20° is taken as an example; the simulation results are shown in Fig. 8.

Figure 8 shows the instantaneous cutting force on the workpiece at 820 step of the simulation. At this time, the cutting process has been stabilized, and the force shows a maximum value and a minimum value. The force on the workpiece is dynamic and varies in different sections of the workpiece, as shown in the diagram. Because machining is a continuous operation, the instantaneous cutting force cannot describe the cutting force change process over the entire cutting process. To test the efficiency of the simulation model, extract the maximum value of the cutting force from these phases, then take the average value of the extracted maximum cutting force, and compare it to the maximum cutting force acquired from the experiment. The highest cutting force value in the simulation process is extracted using the step-average method in this study. Specifically, every 50 steps, the greatest cutting force is retrieved, and the extracted maximum cutting force is then averaged to give a more accurate cutting force value under simulation settings.

## 3 Experimental work

The experiment is carried out in Xi'an Precision Mechanical Engineering Co., Ltd, and the experimental equipment information is shown in Table 4. The data acquisition rate is about 20,000 samples per second, as shown in Figs. 9 and 10. The workpiece is made of 7075-T6 aluminum alloy bar, which has a size of Φ150 mm × 60 mm, after solution treatment and pre-stretching treatment. In order to reduce the influence of clamping force on the deformation of the component, the upper part of the workpiece is machined into a square of 100 mm × 100 mm × 35 mm, and then divided into 25 pieces of 12 mm × 12 mm × 2 mm. Two bolts secure the lower half of the workpiece to the dynamometer, and two pressing plates secure the dynamometer to the machine tool workstation. The dimension drawing and installation drawing of workpiece after machining are shown in Fig. 11.

## 4 Results and discussions

Figure 12 shows the cutting force curve under the cutting condition of $n = 20{,}000$ rpm, $f = 50$ mm/s, $a_p = 0.1$ mm, $a_w = 0.5$ mm, $\alpha = 20°$.

The cutting force curve, as shown in Fig. 12, has 36 periodic peaks and valleys, each cycle representing a groove made by the tool on the surface, which can be separated into three stages:

The dynamometer has started to work for sampling, but the tool has not yet made contact with the workpiece; therefore, the cutting force is displayed as zero in the first stage, 0–20 s.

The second stage is the tool cutting stage, 20–60 s; the tool has cut into the workpiece; the dynamometer has displayed the curve of cutting force. The curve has peaks and valleys, which appear alternately. The peaks are the stage when the tool is cutting, while the valleys are the stage when the tool cuts out the workpiece and the tool is lifting and moving.

The third stage is the tool cutting out stage, 60–65 s; the tool has cut out the workpiece, which means that the cutting force gradually decreases to zero, and the whole cutting process ends.

Figure 13 shows the cutting force data curve of one cycle of cutting force, which is the cutting force when cutting a groove. Using the *X*-direction cutting force as an example,

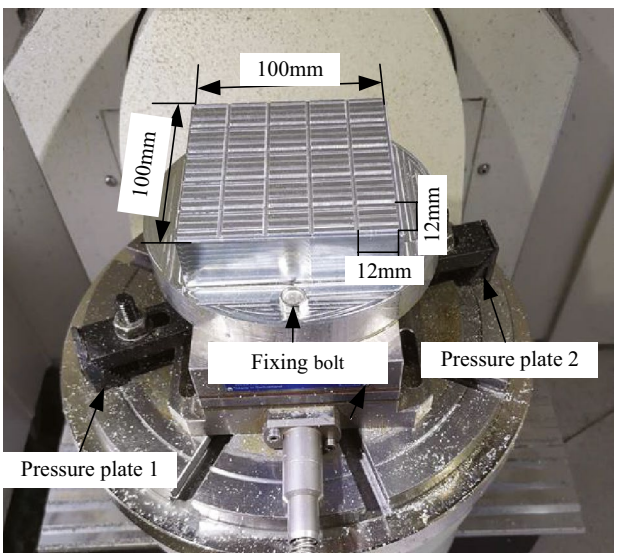


**Fig. 11** Workpiece structure size and installation diagram

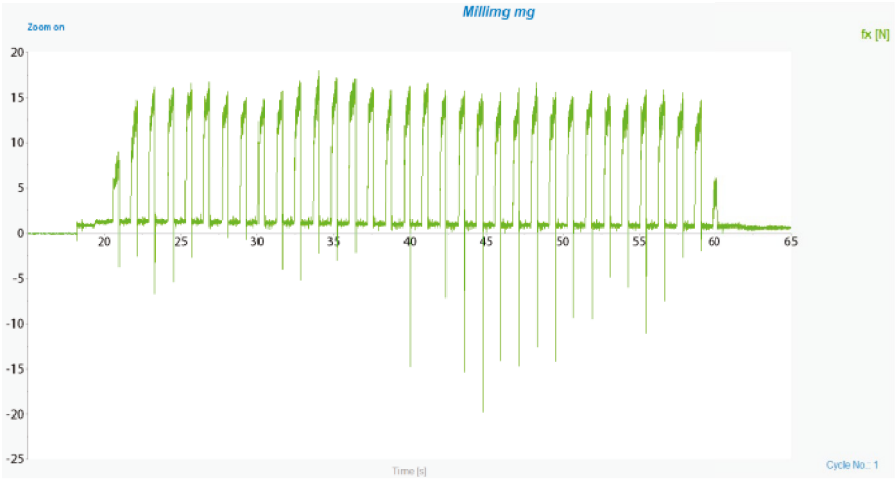


**(a)** Fx data curves

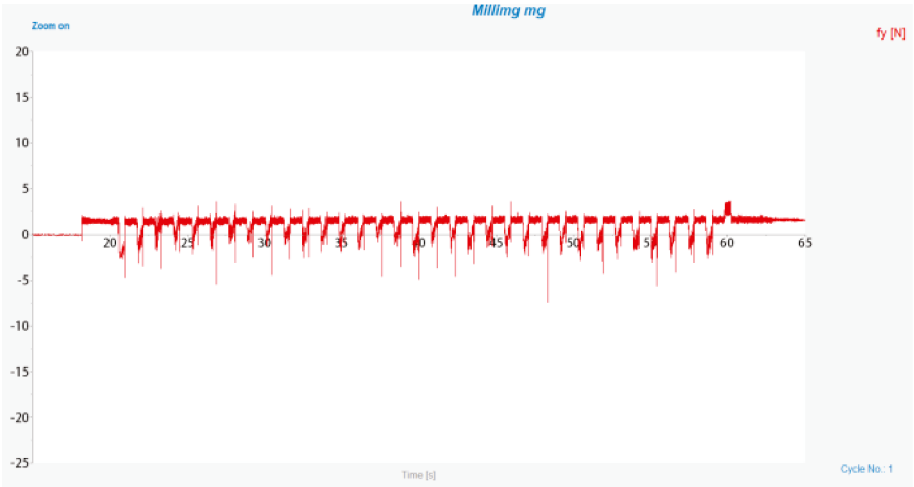


**(b)** Fy data curves

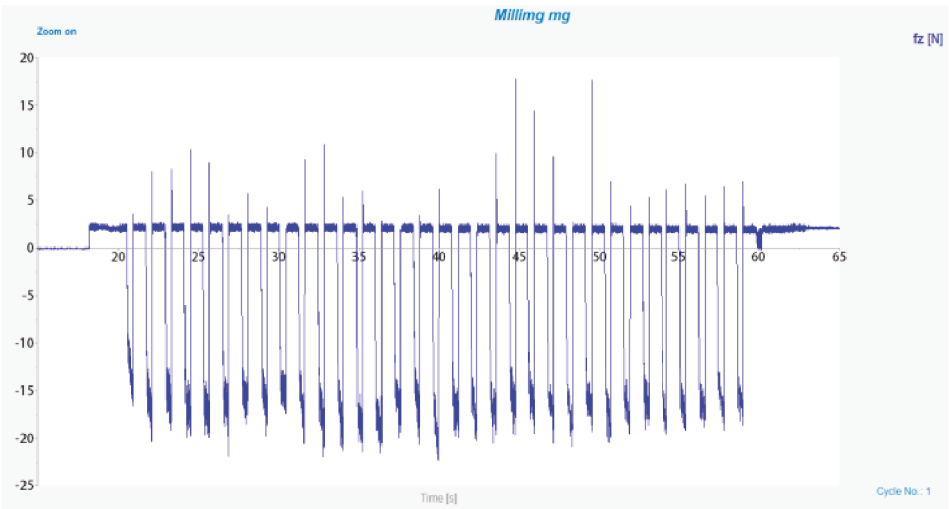


**(c)** Fz data curves

**Fig. 12** Measured cutting forces for the 20° of rake angle. **a** Fx data curves. **b** Fy data curves. **c** Fz data curves

we can examine how the cutting force changes. The cutting force progressively increases from zero to maximum value, then stabilizes, generating an oscillation curve within a specific range. Because the two cutting edge tools' cutting edges alternate, and there is a chip removal groove between the two cutting edges that does not participate in the cutting process. The cutting force curve abruptly changes at the end of cutting, reversing the beginning cutting force. This is because the metal cutting process is the extrusion process between the tool and the material, and then, the material has elastic–plastic deformation. Finally, after reaching the limit value of material fracture, the part of the material will leave the body material in the form of chips. The other part of the material has elastic deformation, when the extrusion of the tool disappears, it will rebound and produce a force, which is just opposite to the cutting force. The analysis process of the other two directions is similar to $F_X$.

The average cutting force in the simulated cutting process is compared to the average cutting force measured in the experiment to ensure that the finite element model is correct. In Fig. 14, the simulated average cutting force values under different rake angles are plotted with the red line with dots, and the measured average cutting force values are plotted with the black line with squares. The description forms in Figs. 15 and 16 are identical to the above statements.

The simulation data of the force value ($Fx$) in the radial ($X$) direction is more consistent with the size distribution of the experimental data, as shown in Fig. 14, and the trend of the simulated cutting force is in good agreement with the experimental data. As the rake inclination angle increases, the change range of $Fx$ first increases and then decreases, and finally tends to be stable. In the range of 12 ~ 22°, the cutting force shows a trend of first increasing and then decreasing, and the maximum value of cutting force is 22.2 N at 20°. In the range of 22 ~ 32°, the cutting force also shows a trend of first increasing and then decreasing, and the maximum value of cutting force is 19.27 N at 28°. After the rake inclination angle of 34°, the cutting force tends to be stable without major fluctuations.

Figure 15 shows that the overall data distribution shows that the simulated data of cutting force ($Fy$) in the feed ($Y$) direction has a comparable variation pattern to the experimental data. The fluctuation trend of $Fy$ in the process of increasing the rake angle is not as severe as that of $Fx$ and $Fz$, which is reasonably stable, and the force in the feed direction is the smallest when compared to the cutting force in the $X$ and $Y$ directions.

Figure 16 shows that in comparison to the $X$ and $Y$ directions, the cutting force in the $Z$ direction is the greatest, and the error between simulation and experimental data in this direction is the greatest, but the general trend is similar. With the increase in the rake angle, the peak value of the fluctuating cutting force becomes smaller and more stable. In the range of rake angle of 12 ~ 22°, $Fz$ increases at first and then decreases sharply. When the rake angle is 20°, the cutting force test value reaches the maximum value of 23.33 N. In the range of

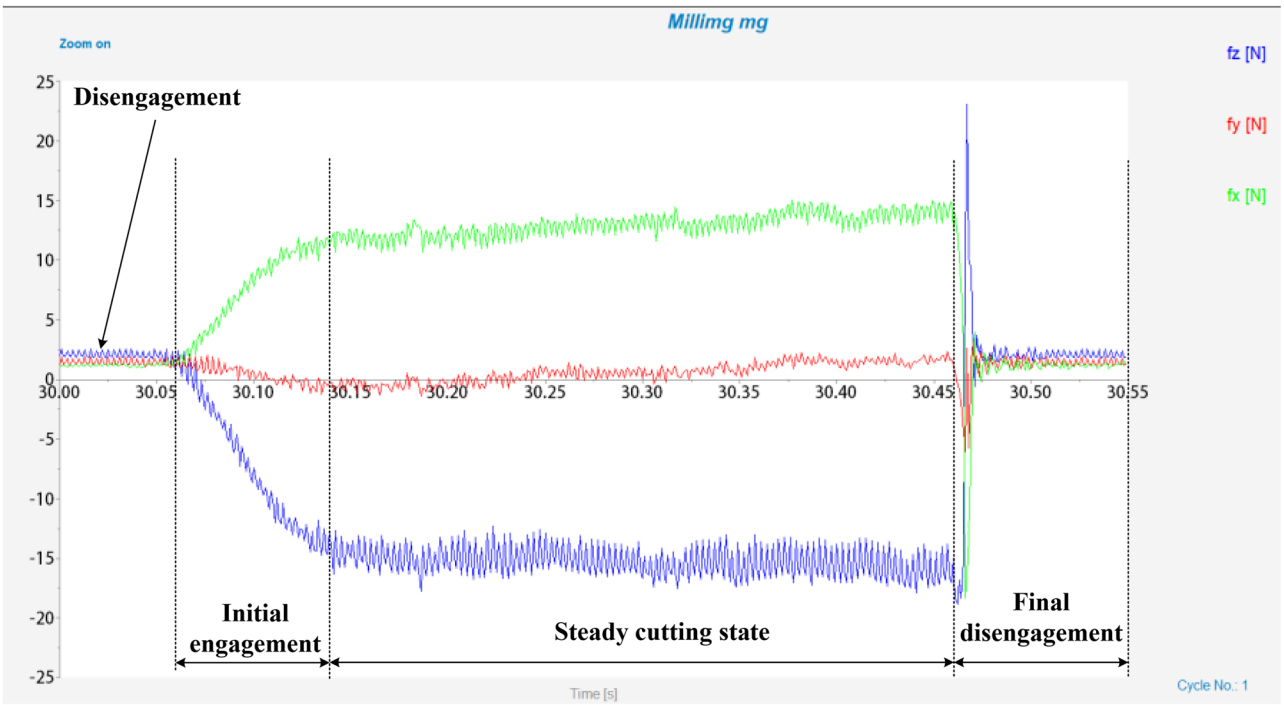


**Fig. 13** Experimental data curve of cutting force in each direction for one cycle

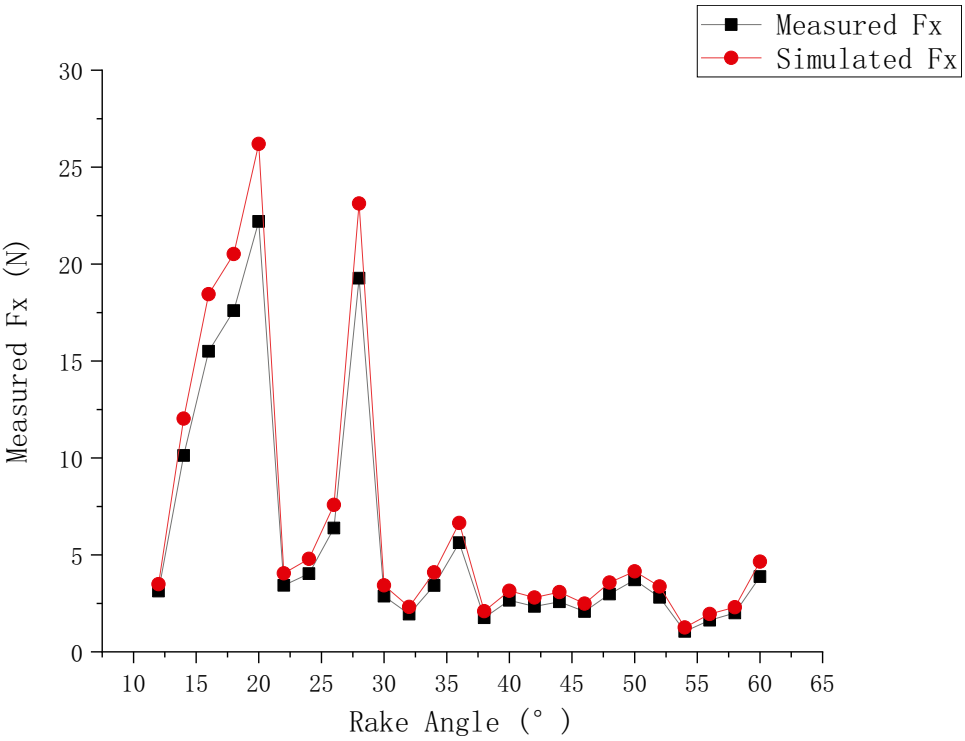


**Fig. 14** Comparison of cutting forces between simulation and experiments under *Fx*

rake angle of 22 ~ 32°, the maximum value of cutting force is 17.23 N at 28°. At a rake angle of 32 ~ 42°, the cutting force also increases at first and subsequently drops, with the maximum value of 12.50 N in the 36° range. The peak value of the fluctuation of cutting force is stable after a rake angle of 42°.

Although the cutting force simulation results in various directions and the experimental findings have some flaws, the overall trend of the cutting force obtained by simulation with the inclination angle is compatible with the experimental data. Considering the slight differences between the

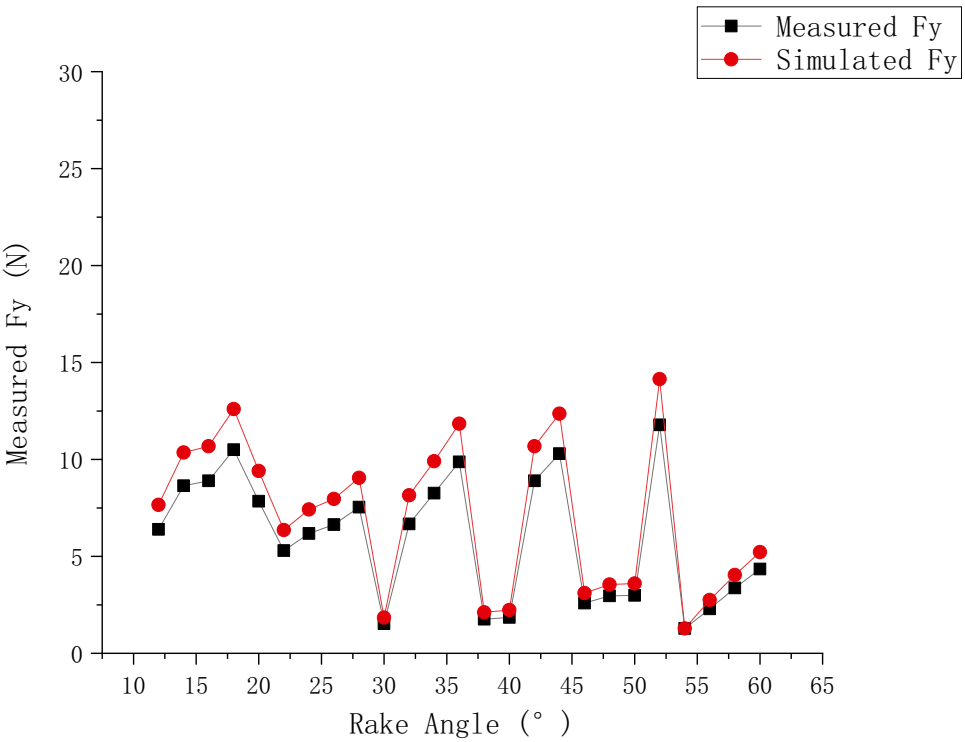


**Fig. 15** Comparison of cutting forces between simulation and experiments under *Fy*

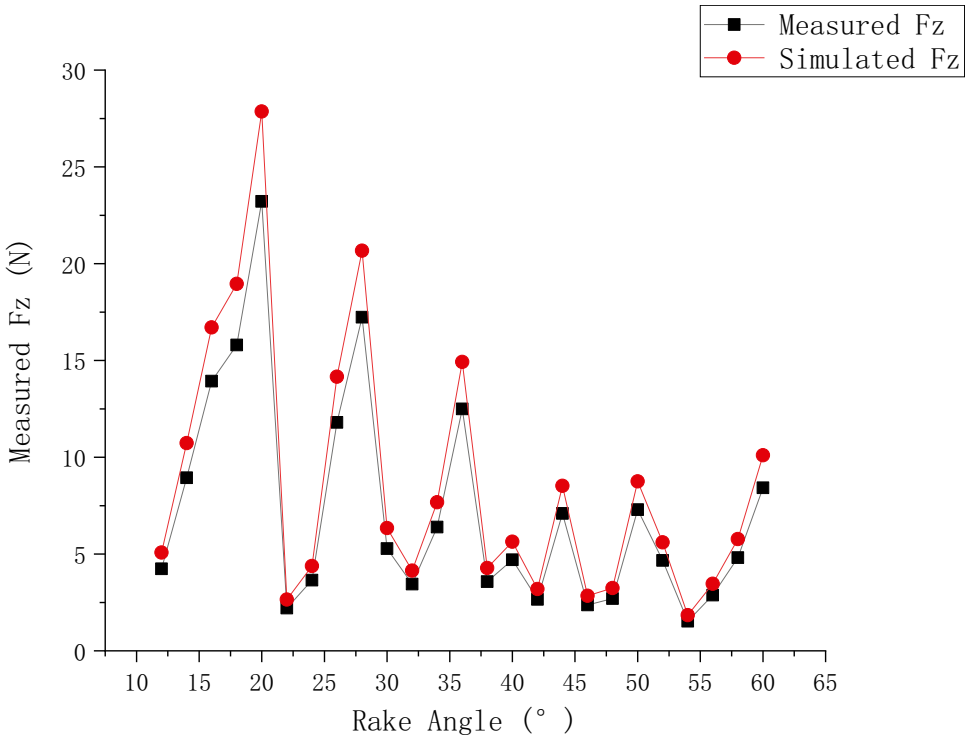


**Fig. 16** Comparison of cutting forces between simulation and experiments under *Fz*

actual processing environment and the simulation processing environment, the main factors are the environmental temperature and mechanical vibration, as well as the error of data acquisition; the error of about 20% is controllable. The force distribution and the trend of the main cutting force are basically consistent between the simulation and the test, which shows that the best result of the simulation is proved by the experiment, and the simulation prediction is reliable and has a certain practical engineering application value. Based on the research of other scholars, the simulation and experimental data of the inclination angle change in this study were more sufficient than the literature [18, 18], so the optimal machining inclination angle obtained was more accurate. Compared with the studies in [20, 20], this study quantified the non-horizontal motion of the tool in multi-axis ball nose milling by the inclination angle between the tool and the workpiece, and established a mapping relationship between the inclination angle and the cutting force. The three-dimensional finite element dynamic simulation model of cutting force established in this study was easier to calculate than the analytical cutting force prediction model of the literature [22].

It can be seen from the above description that in five-axis machining, in order to avoid deformation of the workpiece caused by excessive cutting force, in the case of no interference and super-path, the rake angle should be selected as far as possible to avoid the angle with large cutting force or try to choose a range of rake angle where the cutting force changes more steadily.

## 5 Conclusion

The research develops a three-dimensional finite element dynamic simulation model that properly represents the cutting force of a ball-end cutter used in high-speed milling.

1. The model takes into account not only the actual size of the ball-end milling cutter, but also the rotational movement and intermittent cutting of the tool during the milling process, which is more accurate in reflecting changes in cutting force during high-speed milling and is closer to the actual situation of ball-end milling.

2. A ball-end milling simulation is performed for 25 groups of aluminum alloy 7075 with varied rake angles using the Lagrangian incremental, and the maximum cutting force value in the simulation process is derived using the step-average technique.

3. The cutting force of the simulation is compared to the data acquired from the real verification experiment. The general shifting trend of the simulated maximum cutting force in the feed, radial, and *Z*-direction is similar to the experimental observed value. Because of the difference between the simulation environment and the actual machining environment, there is some inaccuracy between the simulation result and the experimental result; nevertheless, the error can be within acceptable limits.

4. It also suggests a finite element modeling of a sophisticated ball head multi axis milling operation. The findings of modeling and experiment reveal that the rake inclination angle should be avoided as much as possible to be about 22°, 28°, and 36°, and can be taken as 12 ~ 18°, 22 ~ 26°, 30 ~ 34°, and 38 ~ 60°, to obtain a lower and more consistent cutting force. The study result provides superior guiding value for the cutter inclination angle selection and adjustment for multi-axis milling machining.

**Author contribution** Zhijie Wang performed the data analyses and wrote the manuscript; Yan Cao contributed to the conception of the study; Hui Yao contributed significantly to analysis and manuscript preparation; Fan Kou performed the experiment.

**Funding** This research is supported by Xi'an Science and Technology Project (Grant: 2020KJRC0032), Yulin Science and Technology Project (Grant: 2019–122), Project of Joint Postgraduate Training Base of Xi'an Technological University, and Research Project of Graduate Education and Teaching Reform of Xi'an Technological University in 2017.

**Availability of data and material** Not applicable.

**Code availability** Not applicable.

## Declarations

**Ethics approval** Not applicable.

**Consent to participate** Not applicable.

**Consent for publication** Not applicable.

**Conflict of interest** The authors declare no competing interests.

## References

1. Wei ZC, Li SQ, Guo ML et al (2019) Plane surface milling force prediction with fillet end milling cutter under pre-determined inclination angle. Int J Adv Manuf Technol 103(9):2849–2864
2. Guo M, Wei Z, Wang M et al (2018) An identification model of cutting force coefficients for five-axis ball-end milling. Int J Adv Manuf Technol 99(1–4):937–949
3. Buj-Corral I, Ortiz-Marzo JA, Costa-Herrero L et al (2019) Optimal Machining Strategy Selection in Ball-End Milling of Hardened Steels for Injection Molds. Materials 12(6):1–14
4. Dai Y (2019) Research on prediction method of stability lobe diagram for ball-end mill based on engagement. J Mech Eng 55(1):52–61
5. Wei ZC, Guo ML, Wang MJ et al (2018) Prediction of cutting force in five-axis flat-end milling. Int J Adv Manuf Technol 96(1):137–152
6. Wan M, Zhang WH, Tan G et al (2007) New Cutting Force Modeling Approach for Flat End Mill. Chin J Aeronaut 20(003):282–288
7. Kao YC, Nguyen NT, Chen MS et al (2015) A prediction method of cutting force coefficients with helix angle of flat-end cutter and its application in a virtual three-axis milling simulation system. Int J Adv Manuf Technol 77(9):1793–1809
8. Zuperl U, Cus F (2004) Tool cutting force modeling in ball-end milling using multilevel perceptron. J Mater Proc Technol 153–154(none):268–275
9. Zhou J, Ren J (2020) Predicting cutting force with unequal division parallel-sided shear zone model for orthogonal cutting. Int J Adv Manuf Technol 107(3):1–11
10. Luo ZW, Zhao WX, Jiao L et al (2017) Cutting force prediction in end milling of curved surfaces based on oblique cutting model. Int J Adv Manuf Technol 2 89(1–4):1025–1038
11. Sonawane HA, Joshi SS (2010) Analytical modeling of chip geometry and cutting forces in helical ball end milling of superalloy Inconel 718. CIRP J Manuf Sci Technol 3(3):204–217
12. Zdemir M, Ercan K, Büyüker B et al (2021) Analysis of the effect of tool nose radius, feed rate, and cutting depth parameters on surface roughness and cutting force in CNC lathe machining of 36CrNiMo4 alloy steel. J Sci Part A: Eng Innov 8(2):308–317
13. Ehmann KF, Kapoor SG, Devor RE et al (1997) Machining process modeling: a review. J Manuf Sci Eng 119(4):655–663
14. Nishida I, Okumura R, Sato R et al (2018) Cutting force simulation in minute time resolution for ball end milling under various tool posture. J Manuf Sci Eng 140(2):1–6
15. Wang W, Zhang W, Huang D et al (2021) Cutting force modeling and experimental validation for micro end milling. Int J Adv Manuf Technol 117(3–4):933–947
16. Aydin K, Akgün A, Yava A et al (2021) Experimental and numerical study of cutting force performance of wave form end mills on gray cast iron. Arab J Sci Eng 46(12):12299–12307
17. Yue CX, Cai Ch B, Huang C et al (2016) Recent advances in finite element simulation of machining processes. J Syst Simul 28(4):815–825+832
18. Ko TJ, Kim HS, Lee SS (2001) Selection of the machining inclination angle in high-speed ball end milling. Int J Adv Manuf Technol 17(3):163–170
19. Kang MC, Kim KK, Lee DW et al (2001) Characteristics of inclined planes according to the variations of cutting direction in high-speed ball-end milling. Int J Adv Manuf Technol 17(5):323–329
20. Cao Q, Zhao J, Han S et al (2012) Force coefficients identification considering inclination angle for ball-end finish milling. Precis Eng 36(2):252–260
21. Azeem A, Feng HY (2013) Cutting force prediction for ball-end mills with non-horizontal and rotational cutting motions. Int J Adv Manuf Technol 67(5–8):1833–1845
22. Nan C, Liu D (2018) Analytical calculation of cutting forces in ball-end milling with inclination angle. J Manuf Mat Proc 2(2):35–46
23. Duan C, Zhang L (2013) A reliable method for predicting serrated chip formation in high-speed cutting: analysis and experimental verification. Int J Adv Manuf Technol 64(9–12):1587–1597
24. Oh SI, Chen CC, Kobayashi S (1979) Ductile fracture in ax-symmetric extrusion and drawing. J Eng Ind Trans ASME 101(1):36–44